Journal of Magnetism and Magnetic Materials 552 (2022) 169206

Contents lists available at ScienceDirect

Journal of Magnetism and Magnetic Materials

journal homepage: www.elsevier.com/locate/jmmm

The spin-state transition in ACo_2O_4 spinels (A = Be, Mg, Ca, Cd, Zn)

Vyacheslav S. Zhandun *, Oksana N. Draganyuk

Kirensky Institute of Physics - Federal Research Center "Krasnoyarsk Science Centre, Siberian Branch of the Russian Academy of Sciences", 660036 Krasnoyarsk, Russia

ARTICLE INFO

Keywords:
Ab initio calculations
Spinels
Cobalt ion
Oxides
Spin-state transition
Thin films
Pressure

ABSTRACT

The magnetic and electronic properties of the Co-based spinel oxides ACo_2O_4 (A = Be, Mg, Ca, Zn, Cd) were studied within GGA + U approach. It was found that the Co^{3+} ion is in a low-spin state due to the effect of the crystal field of octahedral symmetry. It is shown that Co^{3+} ion undergoes a spin-state transition into the high-spin state under the critical pressure of P = −10 GPa – −20 GPa. This pressure-induced spin-state transition is caused by the redistribution of electrons between the t_{2g}- and e_g-orbitals arising with increasing interatomic distances. The role of interatomic distances between Co^{3+} ion and its ligands is discussed. Thin-film form also favors the appearance of a high-spin state of Co^{3+} ion. At the same critical pressure, there is a sharp increase in the majority spin bandgap and a sharp decrease in the minority spin bandgap. These findings allow manipulating the spin state of Co^{3+} ions and bandgap width through the pressure or strain arising in thin films.

1. Introduction

Transition metal oxides with a spinel structure are of considerable fundamental and applied interest [1-6]. The general configuration of spinel can be written as $A^{2+}B^{3+}{}_2O_4$, where bivalent A-site cations are in the tetrahedral environment of oxygen atoms, and trivalent B-site cations are located in the octahedral sites. These compounds, along with simple structures, have relevant and exciting physical and chemical properties with a wide range of potential applications in modern electronic and spintronic devices [7-12]. For spintronic applications, it is important to be able to control the spins of magnetic atoms by external impacts [13,14] such as light irradiation [15], electric and magnetic fields [16-19], temperature [20], or deformation [21]. Recently, we reported that octahedrally coordinated trivalent Co^{3+} ion in antiferromagnetic semiconductor Co_3O_4 undergoes the spin-state transition from low-spin state to high spin state under pressure [22]. This suggests the possibility of manipulating Co^{3+} spins to control the magnetic properties in other spinels with octahedrally coordinated Co^{3+} ions. In the present paper, we have performed an ab initio investigation of the magnetic and electronic properties of the spinel cobalt oxides ACo_2O_4 and analyzed the ways to control the spin state of Co^{3+} ion and, consequently, the magnetic state of spinel itself.

The most investigated spinel cobalt oxides ACo_2O_4 are ones containing Ca [23-26] and Zn [23,27-29] as A-site cations. First-principles investigations predict $CaCo_2O_4$ to have good stability, low activation energy barrier, and high energy capacity [23,24] that make it a promising candidate Ca-ion cathode material for rechargeable Ca-Ion batteries. $CaCo_2O_4$ having high electrical conductivity is investigated by experimental methods to obtain it as an earth-abundant electrocatalyst for oxygen evolution reaction [25,26]. $ZnCo_2O_4$ synthesized by different methods is also regarded as a lithium-ion batteries anode material due to its stable and high capacities [23,27]. The band structure and density of states based on DFT and subsequent growth of $ZnCo_2O_4$-CNT composite [28,29] show high energy density, low cost, easy preparation, environment friendliness, and multiple application that can be used as electrodes for both supercapacitors and lithium-ion batteries. The most unexplored materials from the investigated list are $MgCo_2O_4$ [30,31], $CdCo_2O_4$ [32], and $BeCo_2O$.

The paper is organized as follows. In Sec. II we give a brief description of the calculation details, in Sec. III.1 the results of structural, magnetic, and electronic properties of the spinel are reported. In Sec. III.2 we discuss the pressure-induced spin-state transition of Co^{3+} ion. In the last Section, we make conclusions.

2. Calculation details

Ab initio calculations were performed using the VASP package [33] with projector augmented wave (PAW) pseudopotentials [34]. The valence electron configuration $3d^74s^2$ was taken for Co atom, $2\ s^2$, $3\ s^2$, $3s^23p^64s^2$, $3d^{10}4s^2$, $4d^{10}5s^2$ configurations were taken for Be, Mg, Ca, Zn and Cd atoms, correspondingly and $2s^22p^4$ was taken for O atoms. The exchange–correlation functional within the Perdew-Burke-Ernzerhoff

* Corresponding author.
E-mail address: jvc@iph.krasn.ru (V.S. Zhandun).

https://doi.org/10.1016/j.jmmm.2022.169206
Received 8 November 2021; Received in revised form 17 February 2022; Accepted 18 February 2022
Available online 21 February 2022

(PBE) parameterization [35] and the generalized gradient approximation (GGA) have been used. The plane-wave cutoff energy 500 eV is taken and 8x8x8 Monkhorst-Pack mesh of special points [36] was used for the Brillouin-zone integration. GGA + U calculations were performed within Dudarev's scheme [37] with U = 4.5 eV for Co ion (following Ref. [38]). Since the experimental reports about a synthesis of $BeCo_2O_4$ spinel are absent, we have checked the phase stability of this compound by comparing the total energy of $BeCo_2O_4$ spinel to that of the set of competitive phases (Be_5Co, Be_3Co, Co_3O_4, CoO, BeO, BeCo, Be, CoO_2, Co, O_2) for the calculation of the phase formation enthalpy [39]. The obtained negative phase formation enthalpy (H_{CP} = −0.014 eV/cell) indicates that $BeCo_2O_4$ is thermodynamically stable.

3. Results and discussion

1. Structural, electronic, and magnetic properties of ACo2O4 spinels (A = Be, Mg, Ca, Cd, Zn)

The spinel structure AB_2O_4 has a face-centered unit cell with space symmetry group *Fd* $\bar{3}$ *m* (Fig. 1a). As mentioned in the Introduction, Co^{3+} ions are located in the center of oxygen octahedrons; A^{2+} ions are located in the center of oxygen tetrahedrons. However, it is experimentally found that $CaCo_2O_4$ crystallizes in the orthorhombic structure with space symmetry group *Pnma* (Fig. 1b), consisting of an edge- and corner-shared CoO_6 octahedral network [40]. Therefore, we have calculated the total energy of both structural types for all compounds to find the lowest energy crystal structure depending on A-site cations. Indeed, it was obtained that $CaCo_2O_4$ prefers orthorhombic structure, while other cobaltites have the cubic structure as the lowest energy structure (Table 1, first column). At that, the increase of the atomic number of A-site cation decreases the difference in energies between structures.

The calculated lattice parameters after full optimization of the geometry are shown in Table 1. The calculated here values are close to the experimental ones for $ZnCo_2O_4$ (a = 8.120 [41] a = 8.1267 Å, 8.1020 Å, 8.1103 Å and 8.1150 Å [42]), $CaCo_2O_4$ (a = 8.789(2) Å, b = 2.9006(7) Å and c = 10.282(3) Å. [40,43]), and $MgCo_2O_4$ (a = 8.09 Å [29] and 8.02–8.12 Å for different thermal treatment temperature [30]) spinels. The fourth and fifth columns of Table 1 show the A^{2+} - O bond lengths in the AO_4 tetrahedrons (d_{tet}) and Co^{3+} - O bond lengths in the AO_6 octahedrons (d_{oct}). As seen, the distances inside the tetrahedrons and octahedrons are changed nonlinearly. So, in $BeCo_2O_4$ distances inside the CoO_6 octahedrons are larger than ones inside BeO_4 tetrahedrons. However, in Mg-based spinel, these distances are practically comparable, while the distances inside the tetrahedrons begin to prevail. In Ca-, Zr-, and Cd-bases compounds the distances inside the CoO_6 octahedrons become less than ones inside oxygen tetrahedrons. At that, the Co^{3+} - O bond lengths are increased more slowly than A^{2+} - O distances. We have also calculated and compared the Co—O and A—O bond orders within the approach suggested in Refs [44]. The sums of bond orders of A-site and Co ions are shown in Table 1. It was obtained that i) The summary bond order (SBO) of the Co ion is one and a half to two times greater than the SBO of the A-site cation; ii) the change of SBO is well correlated with the change of the distances within CoO_6 groups. Thus, CoO_6 octahedra is more rigid bonded than AO_4 tetrahedron, however the bond order decrease with the increase of the atomic number of A-site cation and lattice parameter.

The densities of electronic states and band structures of Co-based spinels are given in Figs. 2 and 3. As seen, all compounds are insulators with an energy bandgap varying from 1.95 eV to 2.67 eV. The bandgap width increases with the decrease of the lattice parameter (Table 1). This behavior is since with a decrease in the lattice constant, the interatomic distance will decrease. As a result, the interatomic interaction increases, and the valence electrons become more bound inside the atom. Consequently, more energy is required to transfer electrons from the valence band to the conduction band, which is reflected in an increase in the bandgap. The densities of states and band structures of all compounds are quite similar. (Since the band structures of all compounds are similar we give them for Mg- and Zn-based cobaltites only). The delocalized d-electrons of Co^{3+} ion form the states near the Fermi energy in the energy range about (-2; 0) eV (filled t_{2g}-states) and (+2; + 4) eV (empty e_g- states). P-electrons of oxygen are delocalized in the wide energy range and hybridize with t_{2g}-electrons of Co^{3+} ions near the Fermi energy. Notice, that the increase of the atomic number of A-site cations leads to the narrowing of the energy region of the density of states. All compounds have the direct bandgap in the X point of the Brillouin zone, where the transition between valence T_{2g} band and conductive E_g band gives a contribution to low-energy absorption.

To obtain the lowest energy magnetic state we have calculated the total energies of ferromagnetic (FM), antiferromagnetic (AFM), and nonmagnetic (NM) phases. As seen from Table 1, all compounds were found to be non-magnetic (The non-magnetic state here means the absence of a magnetic moment on the cobalt ion at T = 0 K). AFM ordering is lower by energy than FM ordering for Mg_2CoO_4, $CaCo_2O_4$, and $CdCo_2O_4$. However, the energy difference between magnetic (AFM or FM) and non-magnetic states is about 1 eV and decreases with an increase in the atomic number of A-site bivalent cation. The reason for the non-magnetic ground state is clear from the simple consideration. An octahedral environment of Co^{3+} ion leads to the splitting of Co^{3+} d-electronic states into lower energy threefold degenerated t_{2g}-states and higher energy twofold degenerated e_g-states. Indeed, as seen from Fig. 2, the Co^{3+} t_{2g}-states are found below the Fermi energy and form the valence band, while e_g-states are located upper by energy and form the conduction band. Crystal field splitting energy between t2g and eg states of Co^{3+} ion is equal to the energy bandgap width (Fig. 2, Table 1). Since Co^{3+} ion has $3d^6$ valence electronic configuration, t_{2g} states are completely occupied by electrons, while the overlying e_g-states are

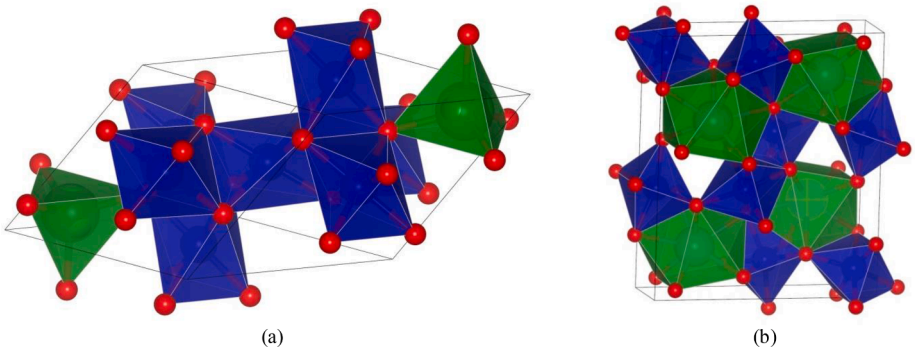

(a) (b)

Fig. 1. (a) Cubic structure (*Fd* $\bar{3}$ *m*); (b) orthorhombic structure (*Pnma*). Blue, green and red colors denote $Co^{3+}O_6$ and XO_4 polyhedra and oxygen atoms, correspondingly.

Table 1
The energy difference between cubic and orthorhombic phases ($\Delta E_{Cub\text{-}Orth}$), calculated lattice parameters, distances inside oxygen tetrahedra (d_{tet}) and octahedra (d_{oct}), the sum of bond order (SBO) of A-site and Co ions, the energy difference between ferromagnetic ($\Delta E_{FM\text{-}NM}$), antiferromagnetic ($\Delta E_{AFM\text{-}NM}$) and non-magnetic phases, energy bandgap (E_g).

	$\Delta E_{Cub\text{-}Orth}$ (eV)	Lattice parameter (s) (Å)	d_{tet} (Å)	d_{oct} (Å)	SBO(A)	SBO(Co)	$\Delta E_{FM\text{-}NM}$ (eV)	$\Delta E_{AFM\text{-}NM}$ (eV)	E_g (eV)
$BeCo_2O_4$	−2.728	7.72	1.71	1.91	1.53	3.06	1.2628	1.5245	2.67
$MgCo_2O_4$	−1.241	8.15	1.96	1,93	1.39	3.00	1.1948	0.8764	2.53
$CaCo_2O_4$	+0.715	8.86	2.24	1.95	1.81	2.89	0.562	0.321	1.95
		2.93							
		10.35							
$ZnCo2O_4$	−2.367	8.15	1.97	1.93	2.28	3.01	1.2556	1.2983	2.45
$CdCo_2O_4$	−1.015	8.43	2.13	1.95	2.44	2.92	1.0143	0.6185	2.29

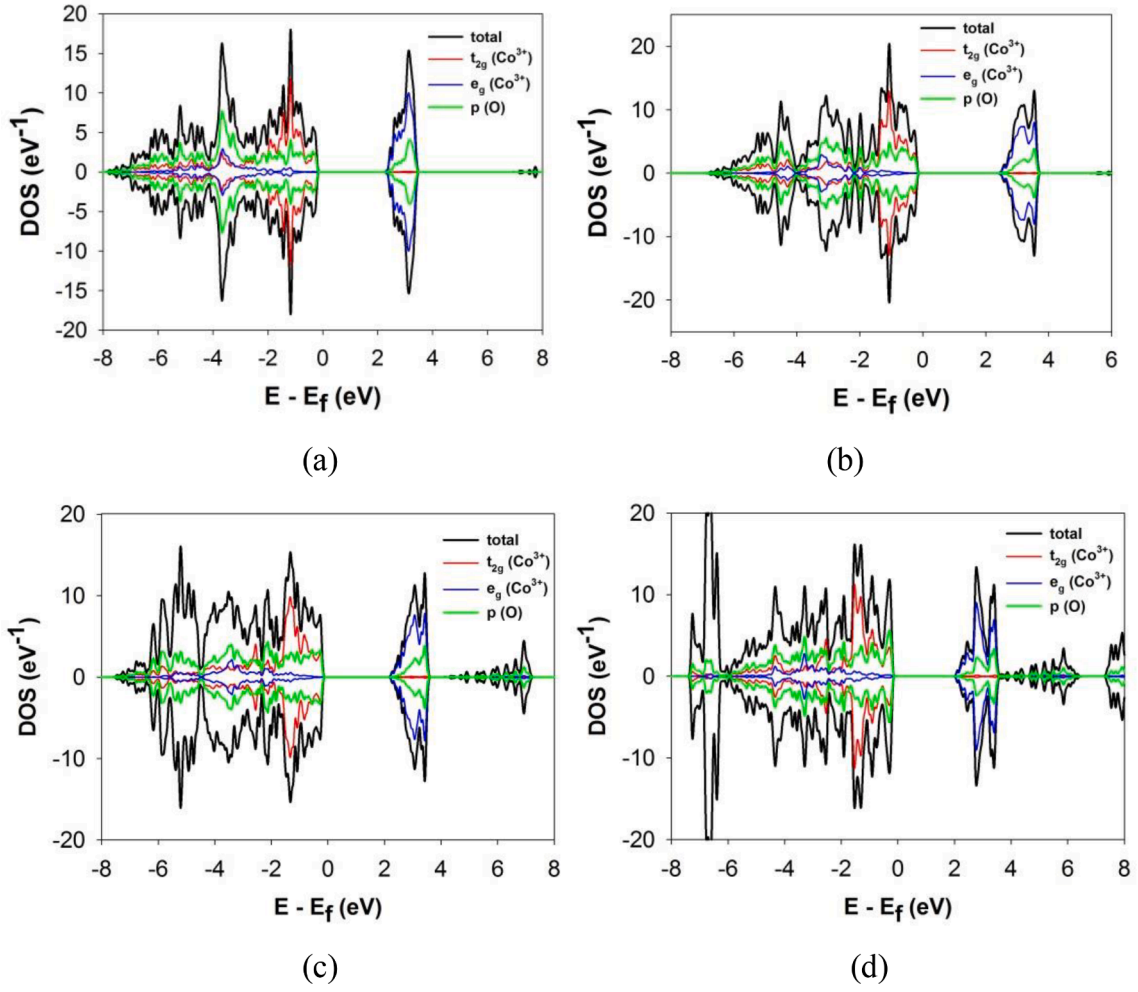

Fig. 2. Total and projected densities of states (DOS) of (a) $MgCo_2O_4$; (b) $CaCo_2O_4$; (c) $ZnCo_2O_4$; (d) $CdCo_2O_4$. The zero on the energy axis is the Fermi energy. Negative values of DOS correspond to the minority spin states.

almost empty. This leads to the appearance of a low-spin state in the Co^{3+} ion and a lowering of non-magnetic state energy in the studied cobaltites.

The question of why the magnetic state becomes more stable with the increasing atomic number of the A-site cation can be considered in terms of Co-O distances inside CoO_6 octahedra. Indeed, the increase of the atomic number of the A-site cation results in the increased distance between Co^{3+} and its nearest neighbors. In turn, this leads to the decrease of crystal electric field caused by oxygen environment and decrease of the crystal field splitting energy (see bandgap width column in Table 1). Since the magnetic state is sensitive to the interatomic distances between Co^{3+} and its oxygen environment, this explains the lowering of the magnetic state energy with the increase of the distances inside $Co^{3+}O^6$ octahedron (Table 1).

2. The pressure-induced spin-state transition of Co^{3+} ion

Let us consider the ways how we can transfer Co^{3+} ions from a low-spin state to a high-spin state. Firstly, it has been suggested that applied pressure can lead to the spin-crossover of Co^{3+} ion from the low-spin state into the high-spin state. To test this hypothesis we have performed the calculation of electronic and magnetic properties of ACo_2O_4 spinels under hydrostatic pressure. Since we need to decrease the splitting between t_{2g} and e_g states (i.e. energy bandgap as we have seen above) to allow d-electrons to occupy high-energy e_g-states, the applied pressure should increase lattice parameter and interatomic distances, i.

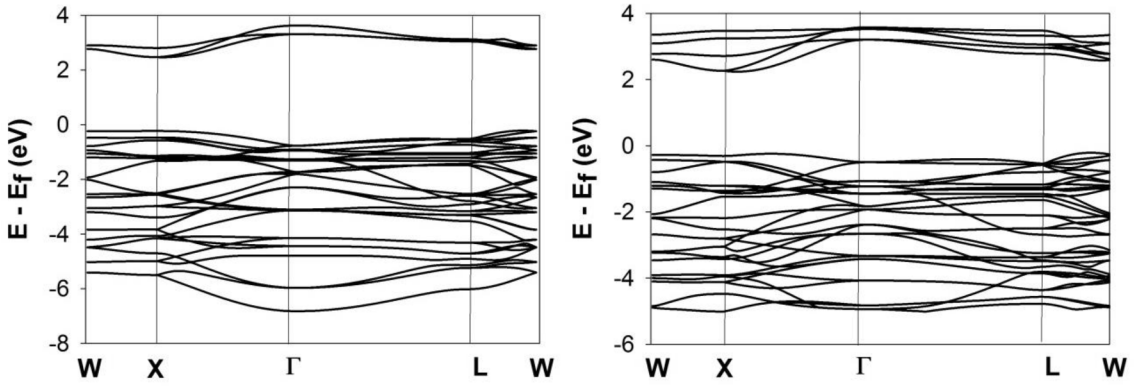

Fig. 3. The band structures of $MgCo_2O_4$ and $ZnCo_2O_4$. Zero corresponds to the Fermi energy.

e. it should be negative. The FM, AFM, and NM configurations were checked as the ground magnetic state. Fig. 4a shows the dependence of magnetic moments on the negative (tensile) pressure. Indeed, at the critical pressure (P = −10 GPa for $CaCo_2O_4$, P = −15 GPa for $MgCo_2O_4$ and $CdCo_2O_4$, P = −20 GPa for $BeCo_2O_4$ and $ZnCo_2O_4$) Co^{3+} ion undergo an abrupt transition from low-spin state to high-spin state with the magnetic moment of about 3μB. The spin state transition observed in Fig. 4a is due to the redistribution of d-electrons between the t_{2g} and e_g orbitals under pressure (Table 2, Fig. 5).

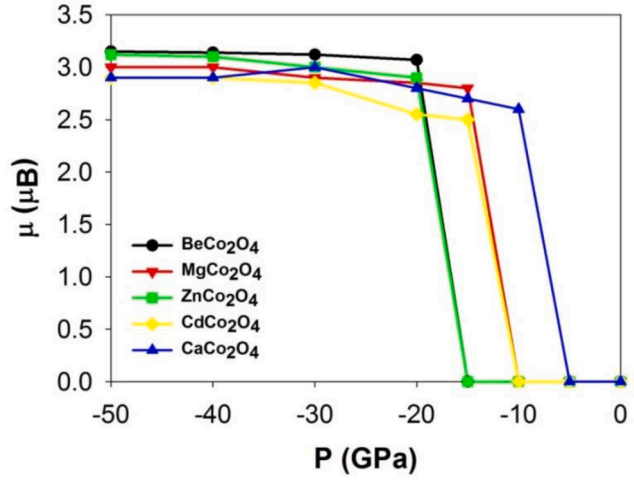

(a)

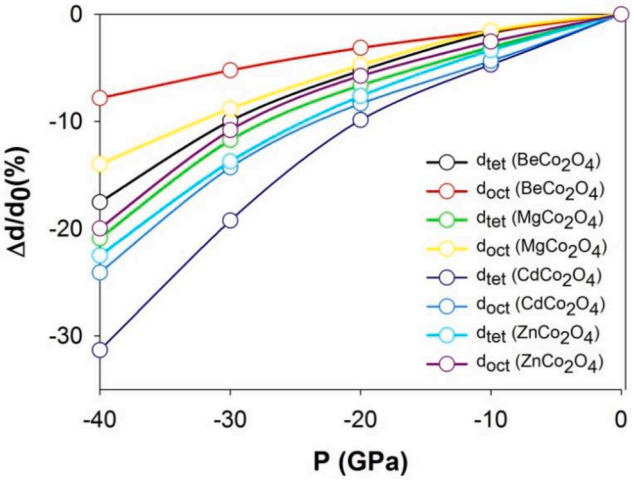

(b)

Fig. 4. (a) The pressure dependence of Co^{3+} ion magnetic moments; (b) The pressure dependence of interatomic distances inside AO_4 tetrahedrons and CoO_6 octahedrons.

Indeed, the magnetic state is sensitive to the interatomic distances between magnetic species and their ligands. As seen from Fig. 4b, the distances inside CoO_6 octahedrons increase with pressure. The distances inside AO_4 tetrahedrons are increased more pronounced than distances inside CoO_6 octahedrons once more suggests stronger bonds between Co and oxygen atoms and agreeing with the results obtained from bond orders analysis (Sec.III.1, Table 1). Note that an increase in the atomic number of A-site cation (i.e. lattice parameter) leads to a more pronounced change in the interatomic distances. An increase in the distances inside the CoO_6 octahedra with pressure leads to a weakening of the crystal field and a decrease in the t_{2g}-e_g splitting. When the critical pressure is reached, the crystal field is reduced so that competing Hund intra-atomic interaction allows the electrons transfer from the filled minority spin t_{2g} - states to the early empty majority spin e_g states (Table 2, Fig. 5), thereby creating a magnetic moment on the Co^{3+} ion. From the structural point of view, this process is similar to the known Jahn–Teller effect induced by strain. We compared the Co-O distances in the NM of and FM phases at the P = −20 GPa and found that these distances are larger in the low-energy FM phase, i.e. it is energetically more favorable to increase the distances within the CoO_6 group. Notice, a similar mechanism of spin-state transition of Co^{3+} ion was also discussed for Co_3O_4 under pressure [45] and strain [46]. The spin-state transition due to the thermal extension was also discussed in $LaCoO_3$ [47] and $GdCoO_3$ [48] under temperature. Following [50] we have estimated the exchange arising between Co ion and its anion environment as follows: $J_{Co,O} = \frac{\Delta E}{\Delta \mu_{Co} \mu_{Co}}$. The obtained results at the pressure of P = 20GPa are: $J_{Co,O}$ = 0.12, 0.24, 0.52, 0.28, 0.48 eV/(μB)^2 for X = Be, Mg, Ca, Zn and Cd correspondingly. As seen, the coupling between Co^{3+} ion and its oxygen environment increase with the increase of the distance within the first coordination sphere of Co^{3+} ion. In addition, the increase of the interatomic distances results in the decrease of the hopping integral t_{ij} between Co and O ions. As it was shown in [49], the small values of hopping integral in the octahedral-coordinated ionic groups contribute to the establishment of magnetic order.

As for the energy bandgap, its dependence on pressure is shown in

Table 2
Occupation numbers of $MgCo_2O_4$ and $ZnCo_2O_4$ under and without applied pressure (P).

P (GPa)	$MgCo_2O_4$				$ZnCo_2O_4$			
	$t_{2g\uparrow}$	$t_{2g\downarrow}$	$e_{g\uparrow}$	$e_{g\downarrow}$	$t_{2g\uparrow}$	$t_{2g\downarrow}$	$e_{g\uparrow}$	$e_{g\downarrow}$
0	0.96	0.96	0.07	0.07	0.95	0.95	0.08	0.08
−20	0.96	0.37	1.0	0.23	1.0	0.37	1.0	0.25

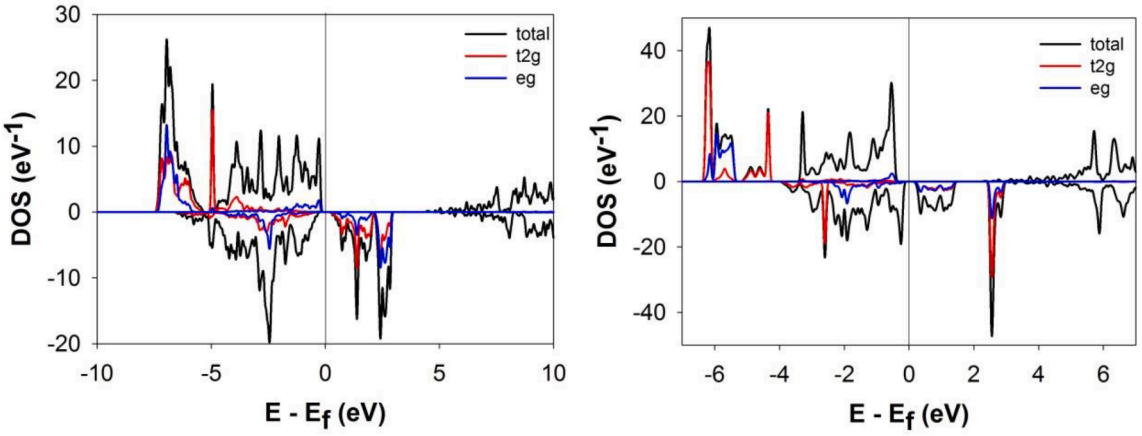

Fig. 5. The total and projected densities of states (DOS) of (a) $MgCo_2O_4$; (b) $ZnCo_2O_4$ under applied pressure P = -20 GPa. The zero on the energy axis is the Fermi energy. Negative values of DOS correspond to the minority spin states.

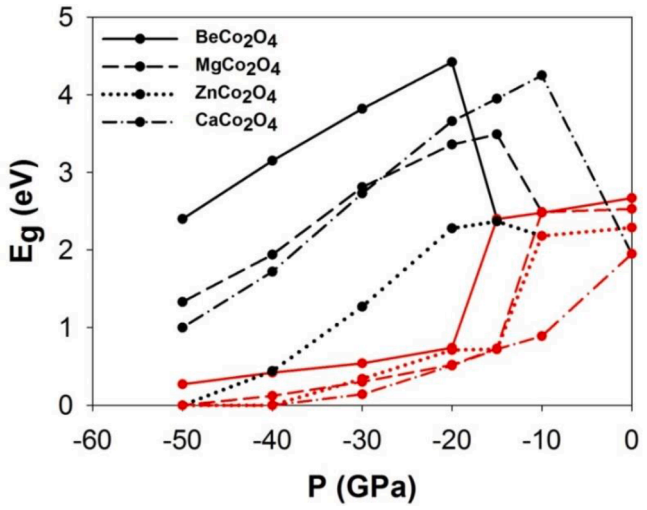

Fig. 6. The pressure dependence of energy bandgaps of $BeCo_2O_4$, $CaCo2O_4$, $MgCo_2O_4$, and $ZnCo_2O_4$ spinels. Black color corresponds to majority spin state bandgaps, the red color corresponds to minority spin state bandgaps.

Fig. 6. At the critical pressure of the spin-state transition from a low-spin to a high-spin state, there is also a sharp decrease in the bandgap for minority spin states. At the same time, the energy bandgap for majority spin states also increases abruptly. With a further increase of the pressure, the bandgap decreases smoothly down to zero. Such behavior of energy band gap under applied pressure is associated with the redistribution of d-electrons between the orbitals under applied negative pressure. As can be seen from Fig. 5, at a pressure above the point of the spin-state transition, the majority spin e_g-states are filled with electrons and shift below the Fermi energy, increasing the energy gap for majority spin states abruptly. At the same time, minority spin t_{2g} states, on the contrary, shift above the Fermi energy, thereby abruptly decreasing the gap for spins down.

Another way to create a high-spin state of Co^{3+} ion in the octahedral site is the fabrication of thin film. We have performed the calculation of the thin film of ACo_2O_4 spinels within slab geometry. The thickness of the thin film was taken as five-unit cells; the vacuum thickness was taken as nine-unit cells. Both the lattice parameters and the internal atomic coordinates of the thin film were optimized for FM, NM, and different AFM and ferrimagnetic states. The ferrimagnetic state with an opposite direction of the magnetic moments in neighbor planes along the c axis turns out to be the lowest in energy for all thin films. The values of magnetic moments vary with the thickness of thin film. Thus, Co^{3+} ions have the maximal value of magnetic moment ($\mu_{max} \sim 3\ \mu_B$) on the surface of thin film and then the magnetic moments decrease deeper into the film. The minimum value (μ_{min} in Table 3) is reached at the center of the thin film. The lattice parameter of the films increased in comparison with the bulk crystal by about 5.5%, after optimization of the thin film geometry (Table 3). This increase corresponds exactly to the tensile stress, which, as was shown earlier, can lead to the transition of the Co^{3+} ion to the high-spin state.

As can be seen from Fig. 7, the density of states of the film is similar to this in a bulk crystal when the tensile pressure is applied (Fig. 5). Thin-film geometry leads to an increase in the lattice parameter and distortions of oxygen octahedrons due to the change of symmetry and surface effects. In turn, this leads to a removal of the degeneracy of t_{2g}- and e_g-states and a decrease of crystal field, and the gap between empty and filled d-states. It is also necessary to take into account the collapse of the crystal field effect in the thin film which could be the result of symmetry change along with that of the pressure. All these processes -results in the splitting and smearing of Co^{3+} electronic density of states. As a result, we observe that the majority of eg-states turn out to be filled and are located below the Fermi energy, while the minority t2g-states, on the contrary, are empty and are located above the Fermi energy. This leads to the appearance of a magnetic moment on Co^{3+} ions and the formation of a magnetic state in thin films (Table 3). This mostly applies to surface and near-surface atoms, where the effect of the surface and hence the symmetry change and distortion of the octahedrons are greatest. Therefore, the magnetic moments of far from surface atoms are less than surface atoms and in some compounds tends to zero (i.e. low-spin state) (Table 3). Notice, the minority spin state bandgap in thin films is closed, while the majority spin state bandgap stays open that forms a half-metal electronic state in the spinel thin films (Table 3).

4. Conclusions

In summary, we have performed the investigation of magnetic and electronic properties of the cobaltite spinels ACo_2O_4 (A = Be, Mg, Ca, Zn,

Table 3
The lattice parameters (a), maximal magnetic moments of Co^{3+} ions (μ_{max}), minimal magnetic moments of Co^{3+} ions (μ_{min}), and bandgaps for the majority ($Eg_\uparrow$) and minority ($Eg_\downarrow$) spin states of spinel thin films.

	$BeCo_2O_4$	$MgCo_2O_4$	$ZnCo_2O_4$	$CdCo_2O_4$
a (Å)	8.17	8.60	8.51	8.97
μ_{max} (μB)	3.1	3.0	2.9	3.0
μ_{min} (μB)	2.7	1.2	1.8	0.9
$Eg_\uparrow$ (eV)	2.15	1.92	1.65	1.21
$Eg_\downarrow$ (eV)	0.00	0.00	0.00	0.00

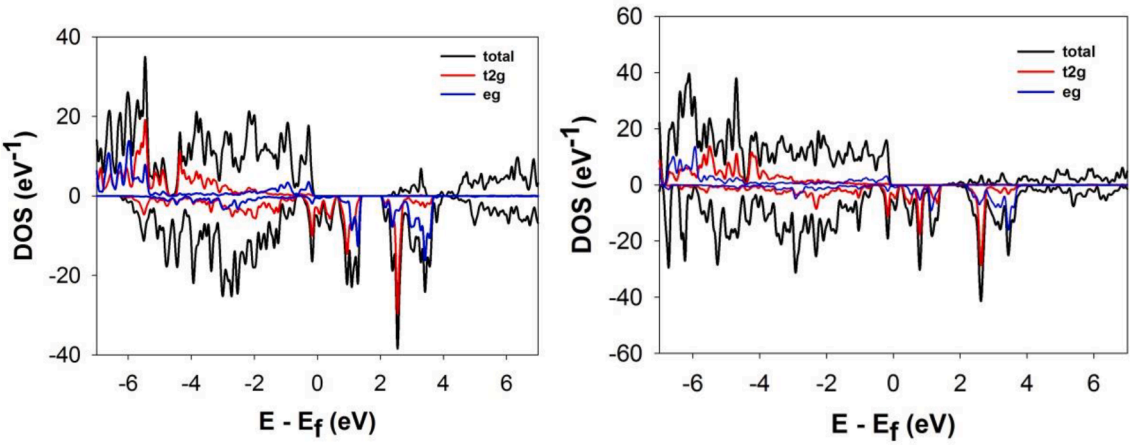

Fig. 7. The total and projected densities of states (DOS) of (a) $MgCo_2O_4$; (b) $ZnCo_2O_4$ thin films. The zero on the energy axis is the Fermi energy. Negative values of DOS correspond to the minority spin states.

Cd). Based on our calculations, all spinels have the cubic unit cell, except for Ca-based spinel which has an orthorhombic structure in agreement with the experiment. The lattice parameter increases with an increase of the atomic number of the A-site cation. In all compounds, the octahedrally coordinated cobalt ion Co^{3+} is in a low-spin state due to the crystal field splitting of t_{2g}- and e_g-states. This leads to all compounds being in a non-magnetic state. We found that the spin state of the Co^{3+} ion and the magnetic state of the spinel can be controlled by pressure. At a critical pressure of about P = -10 – −20 GPa, a sharp appearance of the magnetic moment on Co^{3+} occurs, which corresponds to the spin-state transition of the Co^{3+} ion into the high-spin state due to the redistribution of d-electrons. This pressure-induced spin-state transition leads to the Co-based spinels becoming ferromagnetic. The similar behavior of the Co^{3+} ion was early discussed in $GdCoO_3$ and Co_3O_4 during thermal expansion [48,51]. The formation of low-spin state and high-spin state are discussed in terms of interatomic distances between Co^{3+} ion and its nearest environment. The magnetic (ferromagnetic) state turns out to be favorable by energy in thin spinel films also. All compounds are insulators with the energy band gap varying from 1.95 to 2.67 eV. The applied tensile pressure leads to the abrupt increase of the majority spin bandgap and the decrease of the minority spin band gap at the critical pressure of the spin-state transition. The mechanism of such behavior is related to the shift of the t_{2g}- and e_g-states under applied pressure. Thus, our theoretical predictions can stimulate experimenters and technologists to develop new spintronic materials based on ACo_2O_4 spinels.

CRediT authorship contribution statement

Vyacheslav S. Zhandun: Conceptualization, Methodology, Software, Writing – original draft, Investigation, Data curation, Formal analysis, Writing – review & editing. **Oksana N. Draganyuk:** Software, Investigation.

Declaration of Competing Interest

The authors declare that they have no known competing financial interests or personal relationships that could have appeared to influence the work reported in this paper.

Acknowledgments

The reported study was funded by Russian Foundation for Basic Research, Government of Krasnoyarsk Territory, Krasnoyarsk Regional Fund of Science to the research projects № 19-42-240016: «Control of structural, magnetic, electronic, and optical properties by pressure and intercalation into functional compounds with a spinel structure containing 3d and 4f ions» and № 20-42-240004: "The effect of the composition, pressure, and dimension on the magnetic, electronic, optical, and elastic properties of the magnetic Mn+1AXn (M = Cr, Mn; Fe, A = Al, Ga, Si, Ge, P, In; X = C, N; n = 1-3) MAX-phases". The calculations were performed with the computer resources of "Complex modeling and data processing research installations of mega-class" SRC "Kurchatovsky Institute" (http://ckp.urcki.ru).

References

[1] V. Kocsis, S. Bordács, D. Varjas, K. Penc, A. Abouelsayed, C.A. Kuntscher, K. Ohgushi, Y. Tokura, I. Kézsmárki, Phys. Rev. B 87 (2013), 064416.
[2] V. Fritsch, J. Hemberger, N. Büttgen, E.-W. Scheidt, H.-A. Krug von Nidda, A. Loidl, V. Tsurkan, Phys. Rev. Lett. 92 (2004), 116401.
[3] R. Fichtl, V. Tsurkan, P. Lunkenheimer, J. Hemberger, V. Fritsch, H.-A. Krug vonNidda, E.-W. Scheidt, A. Loidl, Phys. Rev. Lett. 94 (2005), 027601.
[4] D. Santos-Carballal, A. Roldan, R. Grau-Crespo, N.H. de Leeuw, Phys. Rev. B 91 (2015), 195106.
[5] U. Lüders, A. Barthélémy, M. Bibes, K. Bouzehouane, S. Fusil, E. Jacquet, J.-P. Contour, J.-F. Bobo, J. Fontcuberta, A. Fert, Adv. Mater. 18 (2006) 1733.
[6] A. Krimmel, H. Mutka, M.M. Koza, V. Tsurkan, A. Loidl, Phys. Rev. B 79 (2009), 134406.
[7] M. Bibes, A. Barthelemy, Nat. Mater 7 (2008) 425–426.
[8] J.M. Hu, Z. Li, L.Q. Chen, C.W. Nan, Nat. Commun. 2 (2011) 553.
[9] D.D. Awschalom, M.E. Flatt, Nat. Phys. 3 (2007) 153–159.
[10] Z.P. Xing, J.F. Li, D. Viehland, Appl. Phys. Lett. 91 (2007), 142905.
[11] H. Dery, P. Dalal, L. Cywmski, L.J. Sham, Nature 447 (2007) 573–576.
[12] S.E. Shirsath, M.h.n., Xiaoxi Liu, Adnan Younis Assadi, Yukiko Yasukawa, Sumanta Kumar Karan, Ji Zhang, Jeonghun Kim, Danyang Wang, Akimitsu Morisako, Yusuke Yamauchi, Sean Lia, Nanoscale Horizons 4 (2) (2019) 434–444.
[13] S.A. Wolf, D.D. Awschalom, R.A. Buhrman, J.M. Daughton, S. Von Molnar, M. L. Roukes, A.Y. Chtchelkanova, D.M. Treger, Science 294 (2001) 1488–1495.
[14] I. Zutic, J. Fabian, S.D. Sarma, Rev. Mod. Phys. 76 (2004) 323–386.
[15] S. Koshihara, A. Oiwa, M. Hirasawa, S. Katsumoto, Y. Iye, C. Urano, H. Takagi, H. Munekata, Phys Rev Lett 78 (1997) 4617–4620.
[16] H. Ohno, Nat. Mater. 9 (2010) 952–954.
[17] C. Bi, Y.H. Liu, T. Newhouse-Illige, M. Xu, M. Rosales, J.W. Freeland, O. Mryasov, S.F. Zhang, S.G.E.T. Velthuis, W.G. Wang, Phys. Rev. Lett. 113 (2014), 267202.
[18] Q.M. Zhang, Q. Li, R.L. Gao, W.P. Zhou, L.Y. Wang, Y.T. Yang, D.H. Wang, L.Y. Lu, Y.V. Du, Appl. Phys. Lett. 104 (2014), 142409.
[19] K. Sato, A. Matsuo, K. Kindo, Y. Kobayashi, K. Asai, J. Phys. Soc. Jpn. 78 (2009), 093702.
[20] S.W. Biernacki, Phys. Rev. B 74 (2006), 184420.
[21] H. Seo, A. Posadas, A.A. Demkov, Phys. Rev. B 86 (2012), 014430.
[22] V.S. Zhandun, A. Nemtsev, J. Magn. Magn. Mater. 499 (2020), 166306.
[23] H. Park, Y. Cui, S. Kim, J.T. Vaughey, P. Zapol, J. Phys. Chem. C 124 (2020) 5902–5909.
[24] Z. Zhao, J. Yao, B. Sun, S. Zhong, X. Lei, B. Xu, C. Ouyang, Solid State Ionics 326 (2018) 145–149.
[25] X. Lin, J. Zhou, D. Zheng, C. Guan, G. Xiao, N. Chen, J.-Q. Wang, J. Energy Chem. 31 (2018) 125–131.
[26] Linlin Li, Min Ye, Yonghao Ding, Dengyu Xie, Deshuang Yu, Yuxiang Hu, Han-Yi Chen, Shengjie Peng, Journal of Alloys and Compounds, V. 812 (2020) 152099.
[27] J. Bai, X. Li, G. Liu, Y. Qian, Xiong, S. Advanced Functional 24 (2014) 3011.
[28] L. Wu, L. Sun, X. Li, Q. Zhang, H. Si, Y. Zhang, K. Wang, Y. Zhang, Appl. Surf. Sci. 506 (2019), 144964.

[29] W.-W. Liu, M.T. Jin, W.M. Shi, J.G. Deng, W.-M. Lau, Y.N. Zhang, Sci. Rep. 6 (2016) 36717.
[30] D. Darbar, M.V. Reddy, S. Sundarrajan, R. Pattabiraman, S. Ramakrishna, B.V. R. Chowdari, Mater. Res. Bull. 73 (2016) 369–376.
[31] N.L. Okamoto, K. Shimokawa, H. Tanimura, T. Ichitsubo, Scr. Mater. 167 (2019) 26–30.
[32] S. Singh, P. Srivastava, I.S. Kapoor, G. Singh, J. Exp. Nanosci. 10 (2015) 29–44.
[33] G. Kresse, J. Furthmüller, Phys. Rev. B 54 (1996) 11169.
[34] P.E. Blochl, Phys. Rev. B 50 (1994) 17953; G. Kresse, D. Joubert, Phys. Rev. B. 59 (1999) 1758.
[35] J.P. Perdew, K. Burke, M. Ernzerhof, Phys. Rev. Lett. 77 (1996) 3865.
[36] H.J. Monkhorst, J.D. Pack, Phys. Rev. B 13 (1976) 5188.
[37] S.L. Dudarev, G.A. Botton, S.Y. Savrasov, C.J. Humphreys, A.P. Sutton, Phys. Rev. B 57 (1998) 1505.
[38] E. Sasıoglu, C. Friedrich, S. Blügel, Phys. Rev. B 83 (2011) 121101(R).
[39] V.J. Keast, S. Harris, D.K. Smith, Phys. Rev. B 80 (2009), 214113.
[40] M. Shizuya, M. Isobe, E. Takayama-Muromachi, J. Solid State Chem. 180 (2007) 2550–2557.
[41] Y. Sharma, N. Sharma, G.V. Subba Rao, B.V.R. Chowdari, Adv. Funct. Mater. 17 (2007) 2855–2861.
[42] M.V. Reddy, K.Y.H. Ke, J. Electrochem. Soc. 158 (2011) A1423–A1430.
[43] W. Wong-Ng, J. A. Kaduk, & M. Isobe, V. 24 (2009) 343–346.
[44] T. A. Manz, *RSC Adv.*, 7 (2017) 45552-45581; T. A. Manz and N. Gabaldon Limas, Chargemol program for performing DDEC analysis, Version 3.5, 2017, ddec. sourceforge.net.
[45] V.S. Zhandun, A.V. Nemtsev, J. Magn. Magn. Mater. 499 (2020) P.166306.
[46] M.S. Wu, B. Xu, C.Y. Ouyang, Manipulation of spin-flip in Co_3O_4: a first principles study, J Mater Sci 51 (2016) 4691–4696.
[47] M.A. Korotin, S.Y. Ezhov, I.V. Solovyev, V.I. Anisimov, D.I. Khomskii, G. A. Sawatzky, Phys. Rev. B 54 (1996) 5309.
[48] Y.S. Orlov, L.A. Solovyov, V.A. Dudnikov, A.S. Fedorov, A.A. Kuzubov, N.V. Kazak, V.N. Voronov, S.N. Vereshchagin, N.N. Shishkina, N.S. Perov, K.V. Lamonova, R. Yu Babkin, Y.G. Pashkevich, A.G. Anshits, S.G. Ovchinnikov, Phys. Rev. B 88 (2013), 235105.
[49] N.G. Zamkova, V.S. Zhandun, S.G. Ovchinnikov, I.S. Sandalov, J. Alloy. Compd. 695 (2017) 1213–1222.
[50] A.N. Andriotis, M.D. Menon, J. Phys. Condens. Matter 33 (2021), 393002.
[51] V.A.M. Brabers, A.D.D. Broemme, J. Magn. Magn. Mater. 104–107 (1992) 405–406.